Supporting Information for

Vanadium-substituted polycationic Al-oxo cluster in a porous ionic crystal exhibiting Lewis acidity

Wei Zhou,[a] Naoki Ogiwara,*[a] Zhewei Weng,[a] Congcong Zhao,[b] Likai Yan,[b] Yuji Kikukawa,[c] and Sayaka Uchida*[a]

[a]Department of Basic Science, School of Arts and Sciences, The University of Tokyo, Komaba, Meguro-ku, Tokyo 153-8902, Japan

[b]Institute of Functional Material Chemistry, Faculty of Chemistry, Northeast Normal University, Changchun 130024, P.R. China.

[c]Department of Chemistry, Graduate School of Natural Science and Technology, Kanazawa University, Kakuma-machi, Kanazawa, Ishikawa 920-1192, Japan

Table of Contents

Experiment Section

Syntheses. The solution containing $[\delta\text{-}Al_{13}O_4(OH)_{24}(H_2O)_{12}]^{7+}$ (**δ-Al$_{13}$**) was prepared according to our former work[1] as described below. Into 200 mL of water, 12 g of $AlCl_3$ was added (0.45 mol L^{-1} $AlCl_3$(aq)) and stirred at 353 K (solution A). Into 450 mL of water, 4.5 g of NaOH was added (0.25 mol L^{-1} NaOH(aq)), and this solution was slowly added to solution A over 15 min under continuous stirring (pH 3.9). Then, the solution was kept at 368 K for another 2 days (pH 3.8) (denoted as **δ-Al$_{13}$** solution). $K_6PW_9V_3O_{40}\cdot nH_2O$ was synthesized according to a previous report.[2] The ionic crystal (**Al$_{28}$V$_4$-PW$_9$V$_3$**) was synthesized as follows: $K_6PW_9V_3O_{40}\cdot nH_2O$ (0.167 g, 0.06 mol) was dissolved into H_2O (10 mL) to form 6.0 mmol L^{-1} aqueous solution of $K_6PW_9V_3O_{40}\cdot nH_2O$, and 3M HCl was added to the solution under continuous stirring to adjust the pH to 2. Then, 5 mL of 6.0 mmol L^{-1} aqueous solution of $K_6PW_9V_3O_{40}\cdot nH_2O$ (pH = 2) was added to 6 mL of **δ-Al$_{13}$** solution containing NaCl (350 mg, 5.8 mmol), followed by immediate and spontaneous precipitation. The suspension was sealed in a 25 mL glass vessel and kept in an oven at 353 K, and a mixture of orange octahedral-shaped crystals and orange precipitates was produced after 1 week. The product was sonicated, and the suspended impurities were removed by decantation. Distilled water was added to the suspension, and the sonication and decantation process was repeated until the precipitates were completely removed to isolate the orange crystals of **Al$_{28}$V$_4$-PW$_9$V$_3$** (38 mg, 4.5 μmol, yield is 30% based on P). The ionic crystal (**δ-Al$_{13}$-PW$_9$V$_3$**) was synthesized as follows: 5 mL of 6.0 mmol L^{-1} aqueous solution of $K_6PW_9V_3O_{40}\cdot nH_2O$ (pH = 2) was added to 6 mL of **δ-Al$_{13}$** solution containing ethanol (1.2 mL), followed by immediate and spontaneous precipitation. The resulting suspension was kept under ambient conditions, and orange rod-shaped crystals and orange precipitates were produced after 1 day. The crystals of **δ-Al$_{13}$-PW$_9$V$_3$** (30 mg, 7.5 μmol) were isolated using the procedure described in the synthesis of **Al$_{28}$V$_4$-PW$_9$V$_3$** (yield is 25% based on P).

Single crystal X-ray diffraction (SXRD). SXRD data of **Al$_{28}$V$_4$-PW$_9$V$_3$** and **δ-Al$_{13}$-PW$_9$V$_3$** were collected at 153 K with a HyPix-6000 area detector by using a Rigaku Saturn diffractometer with graphite monochromated Mo *K*α radiation (λ = 0.71073 Å). The data reduction and correction were processed with CrysAlisPro software. All the structures are solved by intrinsic phase method (SHELXT[3]) and refined by the full-matrix least-squares method on F^2 using SHELXL-2019/2 crystallographic software package[4] through Olex2[5]. All the atoms were refined anisotropically, and the position of hydrogen atoms on the formic acid is theoretically calculated and refined isotropically. The Platon/Squeeze[6] program was used to mask the electron density of the disordered water molecules and in the voids. The program suggested that 754 (**Al$_{28}$V$_4$-PW$_9$V$_3$**) and 489 (**δ-Al$_{13}$-PW$_9$V$_3$**) electrons exist in the solvent-accessible volume per formula, which were roughly consistent with the amounts of

unassigned water of crystallization in the voids. Crystal data for **$Al_{28}V_4$-PW_9V_3**: orthorhombic *Cmce* (#64), a = 29.9847(5), b = 27.7701(5), c = 23.4604(5), V = 19535.0(6), Z = 4, R_1 = 0.0378, wR_2 = 0.0960, GOF = 1.045. Crystal data for **δ-Al_{13}-PW_9V_3**: orthorhombic *Pnma* (#62), a = 27.8523(4), b = 13.8253(2), c = 25.2206(4), V = 9711.6(3), Z = 4, R_1 = 0.0860, wR_2 = 0.1963, GOF = 1.094. See CSD 2153709 and 2153710 for the crystallographic data of **$Al_{28}V_4$-PW_9V_3** and **δ-Al_{13}-PW_9V_3**, respectively. Table S1 and S2 summarizes the crystallographic data of **$Al_{28}V_4$-PW_9V_3** and **δ-Al_{13}-PW_9V_3**, respectively. BVS (bond valence sum) analyses were performed for the metal atoms (Al and V) using the EXPO2014 program[7], and the results are summarized in Table S4. The protonation sites in **$Al_{28}V_4$** were assigned based on the (i) positive charge of **$Al_{28}V_4$** (+12), which compensates two PW_9V_3 of −6 and the (ii) BVS values and coordination geometry of Al and V atoms. Then, this molecular model was used for the DFT calculation: the geometric structure of **$Al_{28}V_4$** was optimized followed by natural population analysis to obtain the natural charges of the O atoms (see computational details and Table S5).

Characterization. Inductively coupled plasma atomic emission spectroscopy (ICP-AES; Shimadzu, ICPE-9000) was used for the quantitative analysis of inorganic elements (Al, P, W, V). Atomic absorption spectroscopy (AAS) analysis (Hitachi, ZA3000) was used for the quantitative analysis of alkali metals. Prior to the ICP-AES measurement, conc. HNO_3 (1 mL) was added to about 10 mg of the compounds (accurately weighed) to dissolve the solid completely into water (100 mL). According to the elemental analysis and thermogravimetry (Fig. S1), the chemical formula of **$Al_{28}V_4$-PW_9V_3** was determined as follows: $[V_4Al_{28}O_{20}(OH)_{52}(H_2O)_{22}][PW_9V_3O_{40}]_2\cdot 55H_2O$. The chemical formula of **δ-Al_{13}-PW_9V_3** was determined as follows: $[\delta\text{-}Al_{13}O_4(OH)_{24}(H_2O)_{12}][PW_9V_3O_{40}](OH)\cdot 24H_2O$. **$Al_{28}V_4$-$PW_9V_3$** and **δ-$Al_{13}$-$PW_9V_3$** do not contain Na, K by AAS (Na, K) analysis. Ion-exchange chromatography (Cl) showed the amount of Cl in **$Al_{28}V_4$-PW_9V_3** and **δ-Al_{13}-PW_9V_3** is negligible. In previous literature, the compound composed of $[Al_{13}O_4(OH)_{24}(H_2O)_{12}]^{7+}$ and $[H_2W_{12}O_{40}]^{6-}$,[8] which is isostructural with **δ-Al_{13}-PW_9V_3**, was formulated as $[\delta\text{-}Al_{13}O_4(OH)_{24}(H_2O)_{12}][H_2W_{12}O_{40}](OH)\cdot 24H_2O$. Taking together with the result that **δ-Al_{13}-PW_9V_3** contains no Cl^-, we have concluded that **δ-Al_{13}-PW_9V_3** can be formulated as $[\delta\text{-}Al_{13}O_4(OH)_{24}(H_2O)_{12}][PW_9V_3O_{40}](OH)\cdot 24H_2O$. We postulate that OH^- is disordered and cannot be distinguished from the water of crystallization by SXRD analysis due to their similar electron densities. Elemental analysis for **$Al_{28}V_4$-PW_9V_3** (calcd): Al 8.7(8.9), P 0.7 (0.7), W 37.5 (38.8), V 5.9 (6.0). Elemental analysis for **δ-Al_{13}-PW_9V_3** (calcd): Al 8.0 (8.8), P 0.9 (0.8), W 40.6 (41.7), V 4.1 (3.9). Thermogravimetry was conducted with a Thermo Plus 2 thermogravimetric analyzer (Rigaku) with α-Al_2O_3 as a reference under a dry N_2 flow (100 mL min^{-1}) in the temperature range of 303−773 K. X-ray photoelectron spectroscopy (XPS) was

conducted with a KRATOS ULTRA2 (SHIMADZU Corp.) equipped with an aluminum anode (Al $K\alpha$ = 1486.6 eV). Each spectrum was calibrated with the C 1*s* peak at 284.8 eV. Powder XRD patterns were measured with a New ADVANCE D8 X-ray diffractometer (Bruker) by using Cu $K\alpha$ radiation (λ = 1.54056 Å, 40 kV−40 mA) at 1.8 deg min^{-1}. IR spectra were measured by the KBr pellet method with a JASCO FT/IR 4100 spectrometer (JASCO) equipped with a TGS detector. The pyridine-treated **$Al_{28}V_4$-PW_9V_3** sample for IR measurement (Fig. S20) was prepared by mixing ca. 10 mg of **$Al_{28}V_4$-PW_9V_3** with pyridine, subsequently filtering, and drying them under ambient conditions. Solid-state ^{27}Al and ^{51}V MAS NMR spectra were measured with a Bruker AVANCE III 400 WB spectrometer (Bruker) equipped with a 4 mm standard probe operating at 400.18 MHz and a MAS rate of 14 kHz. In the ^{27}Al spectrum, 1M $Al(NO_3)_3$ aqueous solution was used as the external reference with the chemical shift at 0 ppm. In the ^{51}V spectrum, 0.16 M $NaVO_3$ aqueous solution was used as the external reference with the chemical shift at −574.28 ppm.[9] To collect the MAS NMR spectra of **$Al_{28}V_4$-PW_9V_3** treated with 2,6-lutidine or pyridine (Fig. 4), **$Al_{28}V_4$-PW_9V_3** was stirred with 96 equiv. of 2,6-lutidine or pyridine in methanol for 2 h, subsequently filtered, and dried under ambient conditions. N_2 (77 K) and water vapor (298 K) adsorption–desorption isotherms were measured using Belsorp-mini and Belsorp-max volumetric adsorption apparatuses, respectively (Microtac-BEL). Prior to the measurement, about 50 mg of each compound was treated in vacuo at r.t..

Computational details

All density functional theory (DFT) calculations were performed by employing the Gaussian 09 program package.[10] The geometric structure of **$Al_{28}V_4$** was optimized by the hybrid B3LYP exchange-correlation functional.[11] The 6-31G(d) basis set[12] was applied to describe H, O, and Al atoms, while the LANL2DZ effective core potential basis set[13] was used for V atom. Solvent effect of water has been considered using the conductor-like polarizable continuum model (CPCM).[14]

Catalytic Reaction. Acetalization of benzaldehyde was carried out in a glass reactor equipped with a magnetic stirrer. In a typical run, a mixture of benzaldehyde (0.4 mmol), naphthalene (0.1 mmol, internal standard), and catalyst (0.006 mmol) in methanol (2 mL) was stirred under air at 343 K. The reaction progress was followed by gas chromatography using a GC-2014 (Shimadzu) fitted with an InertCap 5 capillary column (GL Sciences) and a flame ionization detector. Solution ^1H NMR spectrum of the filtrate after the acetalization of benzaldehyde with methanol catalyzed by **$Al_{28}V_4$-PW_9V_3** were recorded using a Bruker AV-500 (500 MHz) spectrometer. The acetalization reaction was quenched in the presence of 96 equiv. of 2,6-lutidine or pyridine with respect to **$Al_{28}V_4$-PW_9V_3**. The PXRD patterns of **$Al_{28}V_4$-PW_9V_3** treated with pyridine or 2,6-

lutidine were essentially unchanged from the pristine **$Al_{28}V_4$-PW_9V_3** (Fig. S21), indicating that the crystal structure was maintained after the treatment with pyridine or 2,6-lutidine. The adsorbed amount of pyridine or 2,6-lutidine on **$Al_{28}V_4$-PW_9V_3** was estimated to be 0.29 mol per mol of **$Al_{28}V_4$-PW_9V_3** (N: 0.27wt%) or 0.14 mol per mol of **$Al_{28}V_4$-PW_9V_3** (N: 0.18wt%), respectively, by CHN analysis. The amounts are small due to the relatively weak acid−base interaction, which is still strong enough to quench the reaction, and/or the exposure of the samples to air for a long time (ca. 1 week due to the limited machine time).

Table S1. Crystallographic data of **$Al_{28}V_4$-PW_9V_3**

Empirical formula	$Al_{28}H_{110}O_{229}P_2V_{10}W_{18}$
Formula weight	8410.95
Temperature /K	153.15
Crystal system	Orthorhombic
Space group	*Cmce*
a /Å	29.9847(5)
b /Å	27.7701(5)
c /Å	23.4604(5)
α /°	90
β /°	90
γ /°	90
Volume /Å^3	19535.0(6)
Z	4
ρ_{calc} g/cm^3	2.523
μ /mm^{-1}	11.302
F(000)	13391
Crystal size /mm^3	0.15 ×0.13 × 0.12
Radiation	MoKα (λ = 0.71073)
2θ range for data collection/°	4.922 to 60.108
Index ranges	$-41 \le h \le 38$, $-30 \le k \le 39$, $-24 \le l \le 32$
Reflections collected	70791
Independent reflections	13290 [R_{int} = 0.0493, R_{sigma} = 0.0468]
Data/restraints/parameters	13290/1897/563
Goodness-of-fit on F^2	1.045
Final R indexes [I >=2σ (I)]	R_1 = 0.0378, wR_2 = 0.0960
Final R indexes [all data]	R_1 = 0.0664, wR_2 = 0.1060
Largest diff. peak/hole / e Å^{-3}	1.40/−1.36

Table S2. Crystallographic data of **δ-Al_{13}-PW_9V_3**

Empirical formula	$Al_{13}H_{48}O_{104}PV_3W_9$
Formula weight	3901.56
Temperature /K	153.15
Crystal system	orthorhombic
Space group	*Pnma*
a /Å	27.8523(4)
b /Å	13.8253(2)
c /Å	25.2206(4)
α /°	90
β /°	90
γ /°	90
Volume /$Å^3$	9711.6(3)
Z	4
ρ_{calc} g/cm^3	2.668
μ /mm^{-1}	11.154
F(000)	7196
Crystal size /mm^3	0.15 ×0.14 ×0.10
Radiation	MoKα (λ = 0.71073)
2θ range for data collection/°	4.358 to 60.898
Index ranges	$-29 \le h \le 37$, $-18 \le k \le 19$, $-33 \le l \le 33$
Reflections collected	63808
Independent reflections	13610 [R_{int} = 0.0375, R_{sigma} = 0.0318]
Data/restraints/parameters	13610/2031/525
Goodness-of-fit on F^2	1.165
Final R indexes [I >=2σ (I)]	R_1 = 0.0860, wR_2 = 0.1963
Final R indexes [all data]	R_1 = 0.0930, wR_2 = 0.1991
Largest diff. peak/hole / e $Å^{-3}$	2.62/–3.53

Table S3 Selected bond lengths for **$Al_{28}V_4$-PW_9V_3**

Bond	Length / Å	Bond	Length / Å
W(1)–O(14)	1.701(5)	Al(1)–O(55)#3	1.950(6)
W(1)–O(32)	2.382(5)	Al(1)–O(55)	1.950(6)
W(1)–O(17)	1.887(5)	Al(1)–O(44)#3	1.893(6)
W(1)–O(13)	1.867(5)	Al(1)–O(44)	1.893(6)
W(1)–O(11)#1	1.919(5)	Al(1)–O(33)	1.874(5)
W(1)–O(91)	1.918(5)	Al(1)–O(33)#3	1.873(5)
W(2)–O(32)#1	2.397(5)	Al(2)–O(53)	1.585(9)
W(2)–O(13)	1.907(5)	Al(2)–O(60A)	1.896(15)
W(2)–O(12)	1.887(5)	Al(2)–O(60A)#2	1.896(15)
W(2)–O(11)	1.909(5)	Al(2)–O(60)	1.845(11)
W(2)–O(10)	1.697(6)	Al(2)–O(60)#2	1.845(11)
W(2)–O(8)	1.876(5)	Al(2)–O(54)	1.911(10)
W(3)–O(45)	1.902(6)	Al(3)–O(33)	1.858(5)
W(3)–O(17)	1.924(5)	Al(3)–O(21)	1.934(5)
W(3)–O(18)	1.694(5)	Al(3)–O(25)	1.956(5)
W(3)–O(28)	2.399(5)	Al(3)–O(27)	1.836(5)
W(3)–O(19)	1.882(5)	Al(3)–O(15)	1.847(5)
W(3)–O(12)	1.924(5)	Al(3)–O(23)	1.984(5)
W(4)–O(28)#1	2.412(5)	Al(4)–O(15)#2	1.870(5)
W(4)–O(19)#1	1.906(5)	Al(4)–O(15)	1.870(5)
W(4)–O(61)	1.882(6)	Al(4)–O(35)	1.964(8)
W(4)–O(22)1	1.897(6)	Al(4)–O(24)	1.867(5)
W(4)–O(3)	1.917(6)	Al(4)–O(24)#2	1.867(5)
W(4)–O(2)	1.670(6)	Al(4)–O(16)	1.953(7)
W(5)–O(45)#1	1.963(6)	Al(5)–O(16	1.788(7)
W(5)–O(28)#1	2.407(5)	Al(5)–O(23)	1.820(8)
W(5)–O(5)	1.842(6)	Al(5)–O(31)#2	1.790(5)
W(5)–O(4)	1.636(6)	Al(5)–O(31)	1.790(5)
W(5)–O(22)	1.859(6)	Al(6)–O(47)	1.894(6)
W(5)–O(3)	1.951(6)	Al(6)–O(48)	1.918(6)
W(6)–O(32)#1	2.409(5)	Al(6)–O(27)	1.865(5)
W(6)–O(8)	1.901(6)	Al(6)–O(31)	1.949(5)
W(6)–O(9)	1.940(5)	Al(6)–O(46)	1.886(6)

W(6)–O(6)	1.893(6)	Al(6)–O(34)	1.885(6)
W(6)–O(7)	1.629(6)	Al(7)–O(31)	2.005(5)
W(6)–O(5)	1.898(6)	Al(7)–O(40)	1.847(6)
V(1)–O(44)	1.846(5)	Al(7)–O(1)	1.843(6)
V(1)–O(44)#2	1.846(5)	Al(7)–O(46)	1.894(6)
V(1)–O(21)	2.110(7)	Al(7)–O(37)	1.882(6)
V(1)–O(25)#2	2.005(5)	Al(7)–O(50)	1.940(6)
V(1)–O(25)	2.004(5)	Al(8)–O(26)	1.860(5)
V(1)–O(53)	1.687(8)	Al(8)–O(20)	1.846(5)
V(2)–O(25)#2	1.993(5)	Al(8)–O(31)	2.056(5)
V(2)–O(25)	1.993(5)	Al(8)–O(49)	1.945(6)
V(2)–O(54)	1.765(9)	Al(8)–O(40)	1.839(5)
V(2)–O(47)#2	1.814(6)	Al(8)–O(34)	1.853(6)
V(2)–O(47)	1.814(6)	Al(9)–O(24)	1.867(5)
V(2)–O(23)	2.112(7)	Al(9)–O(41)	1.924(5)
P(1)–O(32)#1	1.529(5)	Al(9)–O(30)	1.852(5)
P(1)–O(32)	1.529(5)	Al(9)–O(26)	1.869(5)
P(1)–O(28)#1	1.534(5)	Al(9)–O(20)	1.855(5)
P(1)–O(28)	1.534(5)	Al(9)–O(16)	2.032(5)

Symmetry operation: #1 1/2–x, +y, 1/2–z; #2 1–x, +y, +z; #3 +x, 1–y, 1–z.

Table S4. Bond valence sum (BVS) for **$Al_{28}V_4$-PW_9V_3**[a]

atom	BVS	atom	BVS
Al1	3.03	Al7	3.08
Al2	2.86	Al8	3.13
Al3	3.08	Al9	3.11
Al4	3.10	V1	4.74
Al5	2.69	V2	4.68
Al6	3.08		

[a] The R_0 and B parameters used were those compiled for Al^{3+} (1.651, 0.37) and V^{5+} (1.803, 0.37) bonded to O^{2-}.[15]

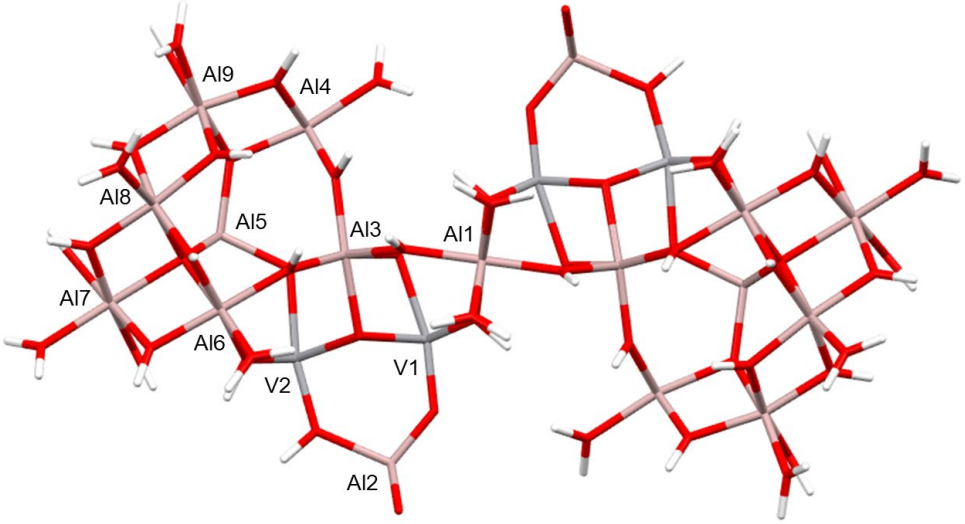

Table S5. Natural charges of representative oxygens in $[V_4Al_{28}O_{20}(OH)_{52}(H_2O)_{22}]^{12+}$

Atomic number	Natural charge	Atomic number	Natural charge
O16 ($Al_2V(\mu_3$-O))	–1.211	O119 (AlV(μ_2-OH))	–0.930
O36 (AlV(μ_2-O))	–0.752	O121 (AlV(μ_2-OH))	–0.965
O37 (AlV(μ_2-OH))	–0.925	O125 (Al(η^1-OH_2))	–0.992
O39 (Al(η^1-O))	–0.705	η^1-$\underline{O}H_2$ of δ-$Al_{12}V^a$	–0.989
O111($AlV_2(\mu_3$-O))	–0.534	μ_2-$\underline{O}H$ of δ-$Al_{12}V^b$	–1.198
O115 ($Al_2(\mu_2$-OH))	–1.205		

Average natural charges of η^1-$\underline{O}H_2^a$ and μ_2-$\underline{O}H^b$ of the non-rotated three $[Al_3O_{13}]$ trimers in the δ-$Al_{12}V$ unit.

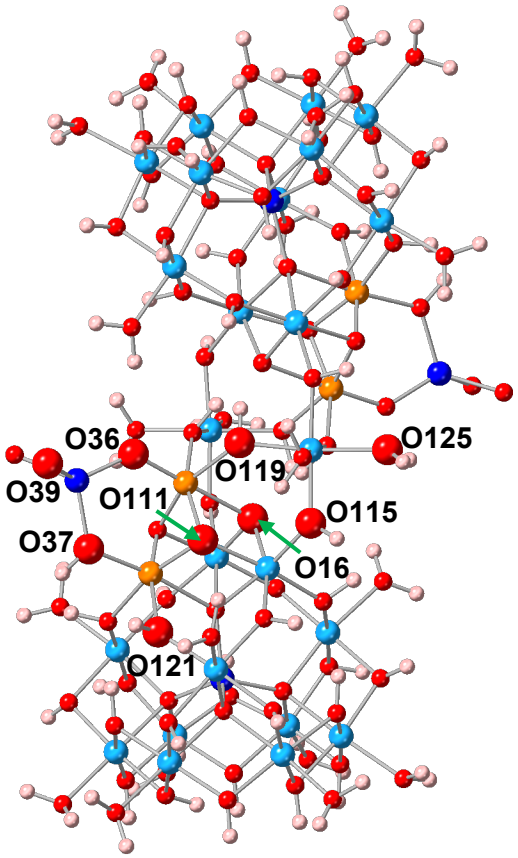

Al atoms in $[AlO_6]$ and $[AlO_4]$ polyhedra are shown in light and dark blue, respectively. V, O, and H atoms are shown in orange, red, and light pink, respectively.

Table S6. Acetalization of benzaldehyde with methanol at 343 K[a]

Entry	Catalyst	Conv.[b] (%)	Yield[c] (%)
1	**$Al_{28}V_4$-PW_9V_3**	53	53
2	**δ-Al_{13}-PW_9V_3**	40	40
3	**δ-Al_{13}-CoW_{12}**	41	41
4	**ε-Al_{13}-CoW_{12}**	39	41
5	**$Al_{28}V_4$-PW_9V_3** (2nd run)	57	57
6	**$Al_{28}V_4$-PW_9V_3** + 2,6-lutidine[d]	54	54
7	**$Al_{28}V_4$-PW_9V_3** + pyridine[d]	36	36
8	$K_6PW_9V_3$	0	0

[a]Reaction conditions: catalyst (0.006 mmol for **$Al_{28}V_4$-PW_9V_3** or 0.012 mmol for Al_{13}-based catalysts and **$K_6PW_9V_3$**), benzaldehyde (0.4 mmol), naphthalene (internal standard, 0.1 mmol), and 2 mL of methanol at 343 K for 2 h. [b]Conversion of benzaldehyde. [c]Yield of benzaldehyde dimethyl acetal. [d]2,6-Lutidine or pyridine was added to the reaction solution after 40 min as a base probe molecule to address the acid sites.

Table S7. Acetalization of benzaldehyde to benzaldehyde dimethyl acetal over various solid catalysts and conditions

Catalyst	Temp [K]	Solvent	Time [h]	Yield[a] [%]	Reference
$Al_{28}V_4$-PW_9V_3	343	methanol	2	53	This work
δ-Al_{13}-PW_9V_3	343	methanol	2	40	This work
$Al(OTf)_3$	ambient	methanol/ orthoester	1	96	1
$Bi(OTf)_3$	reflux	methanol/ trimethyl orthoformate	1	82	2
$CePO_4$	reflux	methanol	6	91	3
Indium MOF	333	methanol	2	76	4
$Cu(BTC)_2$ (MOF)	ambient	methanol	2	63	5
Fe(BTC) (MOF)	ambient	methanol	2	49	5
$Al_2(BDC)_3$ (MOF)	ambient	methanol	24	66	5
UiO-66 (MOF)	301	methanol	24	83	6
$ZnCl_2$	301	methanol	24	39	6
$CoCl_2$	301	methanol	1	34	6
MCM-41(siliceous mesoporous material)	ambient	methanol	24	97	7
Ce-montmorillonite	ambient	methanol	2	49.1	8
Al-montmorillonite	ambient	methanol	2	46.3	8
Fe-montmorillonite	ambient	methanol	2	47.9	8
γ-Al_2O_3	ambient	methanol	2	2.7	8
SiO_2	ambient	methanol	2	0	8
Co–SiO_2	Reflux	methanol	2	99	9
Immobilized IL	353	methanol	1.5	91	10

[a]Yield of benzaldehyde dimethyl acetal. (1) *Green Chem*. 2008, **10**, 914–917. (2) *J. Org. Chem*. 2002, **67**, 5202–5207. (3) *Chem. Sci*. 2017, **8**, 3146–3153. (4) *Chem. Mater*. 2005, **17**, 2568–2573. (5) *Adv. Synth. Catal*. 2010, **352**, 302–3030. (6) *Appl. Catal. A: Gen*. 2015, **506**, 77–84. (7) *Tetrahedron Lett*. 1998, **39**, 9457–9460. (8) *Appl. Clay Sci*. 2011, **53**, 227–235. (9) *J. Iran. Chem. Soc*. 2010, **7**, 695–701. (10) *Adv. Mater. Res*. 2011, **233**, 1336–1339.

Table S8. Pinacol rearrangement at 373K

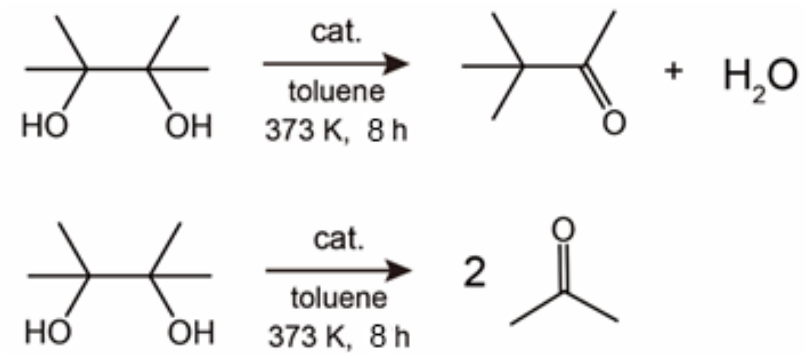

Catalyst	Reaction time (h)	Conv.(%)	Yield of Pinacolone (%)	Yield of Acetone (%)
$Al_{28}V_4$-PW_9V_3	8	100	2	61
δ-Al_{13}-PW_9V_3	8	100	30	22
$K_6PW_9V_3$	8	10	0	11

Reaction conditions: toluene, 2 mL; catalyst, 0.033 mmol for **$Al_{28}V_4$-PW_9V_3** or 0.067 mmol for **δ-Al_{13}-PW_9V_3** and $K_6PW_9V_3$; pinacol, 0.667 mmol; naphthalene (internal standard), 0.267 mmol. Pinacol rearrangement is catalyzed by a mild Lewis acid, and the elimination of water from pinacol (a diol) gives pinacolone (a ketone) via 1,2-methyl shift as a major product. Although both **$Al_{28}V_4$-PW_9V_3** and **δ-Al_{13}-PW_9V_3** exhibited high conversion of pinacol (100%), a large amount of acetone (61% for **$Al_{28}V_4$-PW_9V_3** and 22% for **δ-Al_{13}-PW_9V_3**) was produced by the oxidative dissociation of pinacol, which is probably due to the reduction of vanadium moieties in **$Al_{28}V_4$-PW_9V_3** and **δ-Al_{13}-PW_9V_3**.

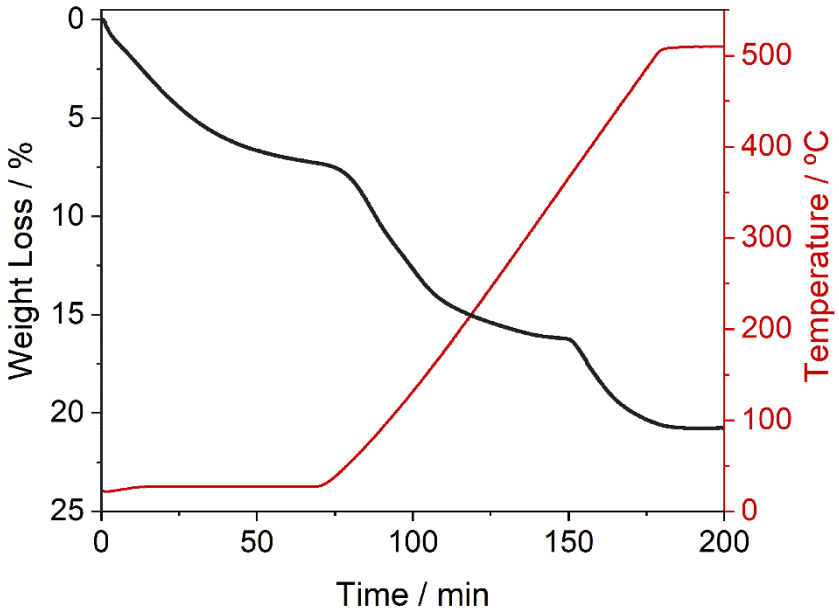

Fig. S1 TGA curve of **$Al_{28}V_4$-PW_9V_3**. The weight loss of 16.3% at 370 °C, where an inflection point is found, roughly corresponds to the loss of the water of crystallization and water molecules coordinated to **$Al_{28}V_4$** ($22H_2O$). The data suggest the existence of 55 molecules of the water of crystallization for **$Al_{28}V_4$-PW_9V_3**.

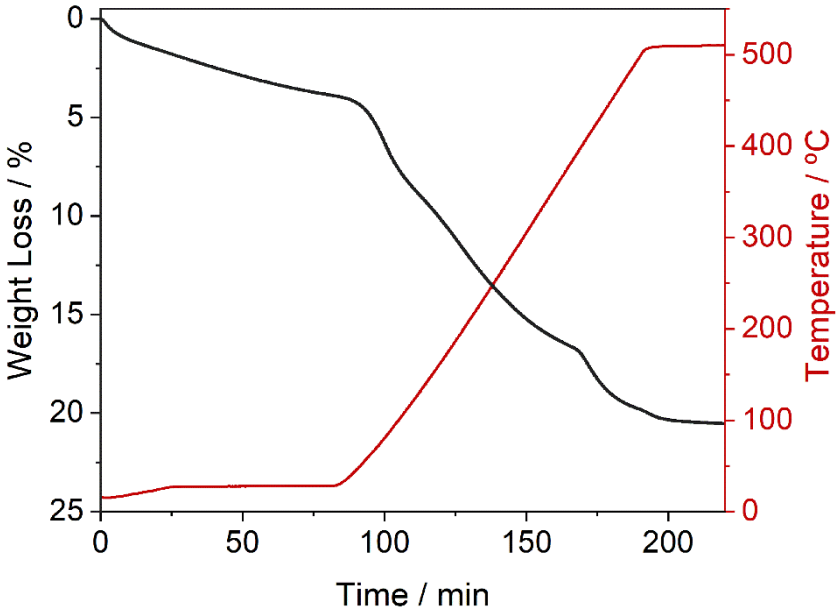

Fig. S2 TGA curve of **δ-Al$_{13}$-PW$_9$V$_3$**. The weight loss of 16.8% at 390 °C, where an inflection point is found, roughly corresponds to the loss of the water of crystallization and water molecules coordinated to **δ-Al$_{13}$** (12H_2O). The data suggest the existence of 24 molecules of the water of crystallization for **δ-Al$_{13}$-PW$_9$V$_3$**.

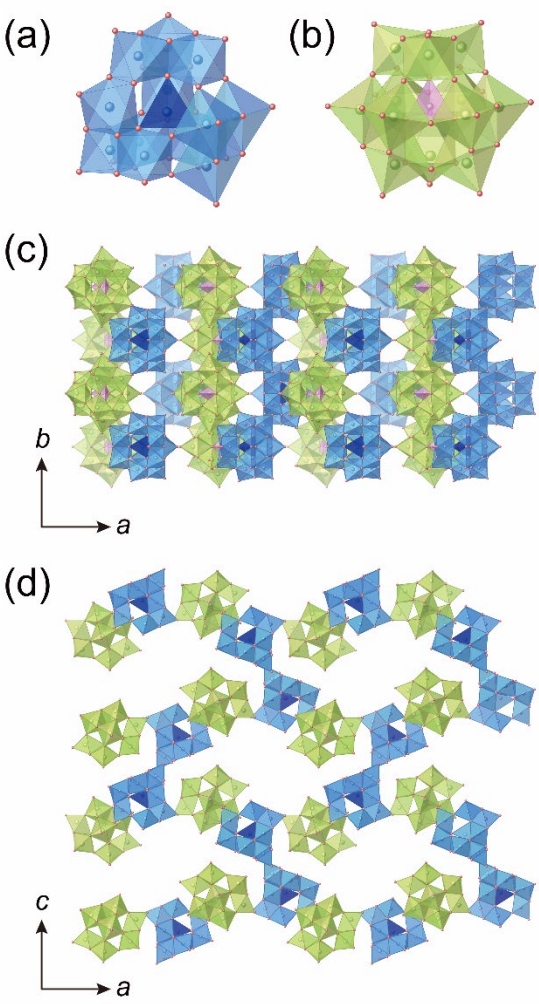

Fig. S3 Local structure of (a) **δ-Al$_{13}$** and (b) **PW$_9$V$_3$**. Crystal structure of **δ-Al$_{13}$-PW$_9$V$_3$** in the (c) *ab*-plane and (d) *ca*-plane. [AlO_6] and [AlO_4] are shown by light blue and dark blue, respectively. [WO_6] and [PO_4] units are shown by light green and pink polyhedra, respectively.

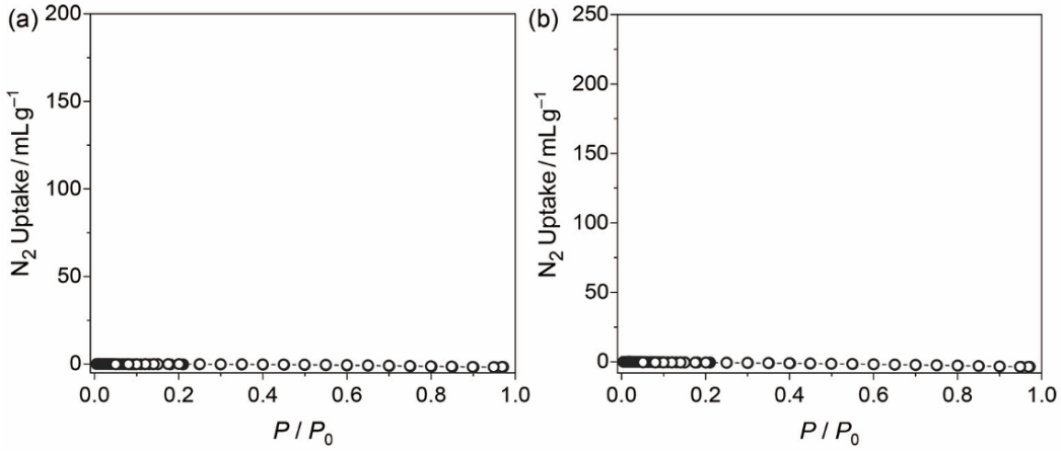

Fig. S4 N_2 adsorption–desorption isotherms (77 K) of (a) **$Al_{28}V_4$-PW_9V_3** and (b) **Al_{13}-PW_9V_3**. Closed and open symbols show the adsorption and desorption branches, respectively. The compounds did not adsorb N_2, probably because porosity is lost by the pretreatment (i.e., evacuation at r.t.).

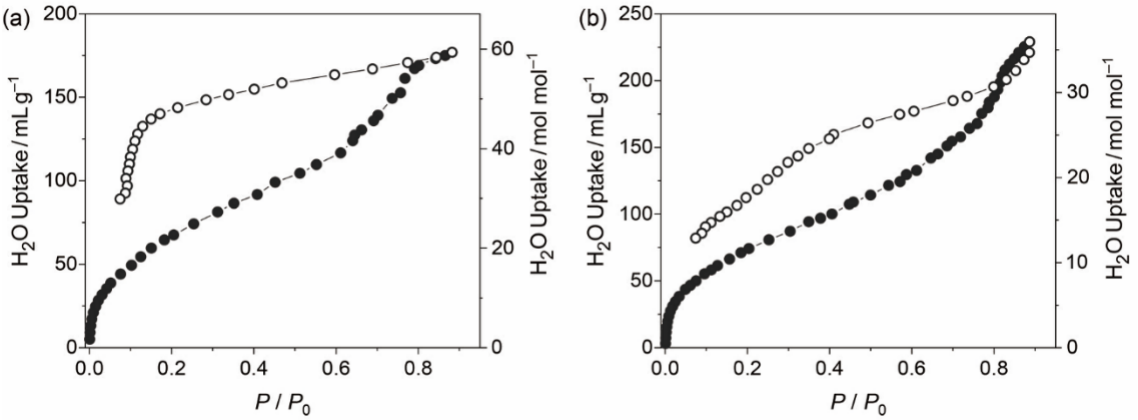

Fig. S5 Water vapor adsorption–desorption isotherms (298 K) of (a) **$Al_{28}V_4$-PW_9V_3** and (b) **Al_{13}-PW_9V_3**. Closed and open symbols show the adsorption and desorption branches, respectively. The compounds adsorb water, and the amounts of water uptake at high relative pressures (ca. 60 and 30 mol mol^{-1} at $P/P_0 = 0.8$ for **$Al_{28}V_4$-PW_9V_3** and **δ-Al_{13}-PW_9V_3**, respectively) fairly agreed with the amounts of the water of crystallization (55 and 24H_2O for **$Al_{28}V_4$-PW_9V_3** and **δ-Al_{13}-PW_9V_3**, respectively).

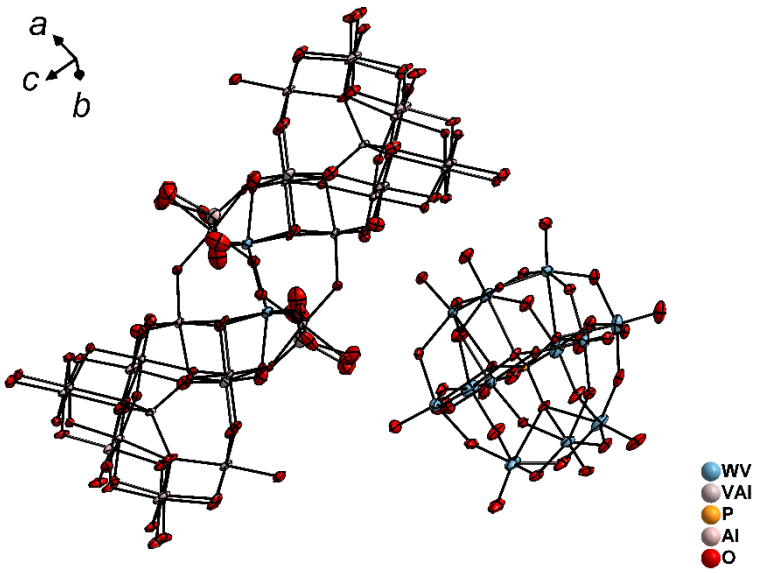

Fig. S6 ORTEP drawing of **$Al_{28}V_4$-PW_9V_3** showing thermal ellipsoids at the 50% probability level.

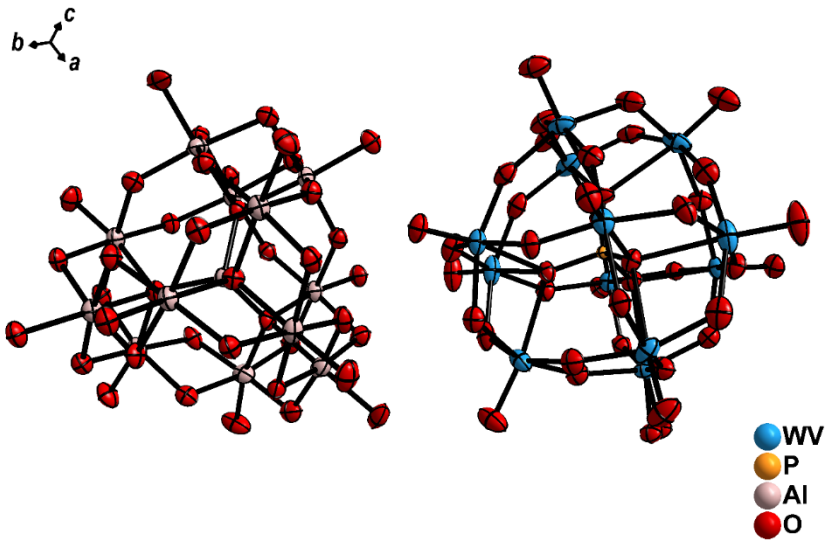

Fig. S7 ORTEP drawing of **δ-Al_{13}-PW_9V_3** showing thermal ellipsoids at the 50% probability level.

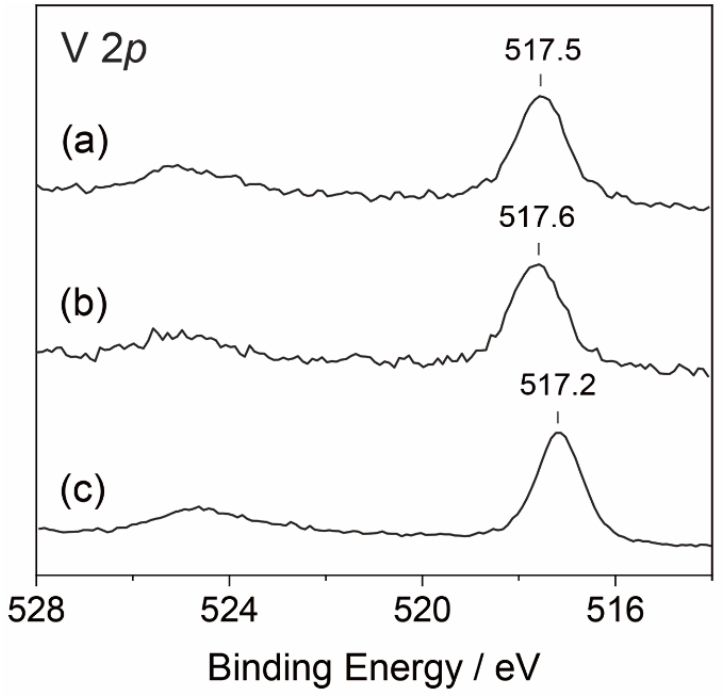

Fig. S8 XPS V 2p spectra of (a) **$Al_{28}V_4$-PW_9V_3**, (b) **δ-Al_{13}-PW_9V_3**, and (c) $K_6PW_9V_3$.

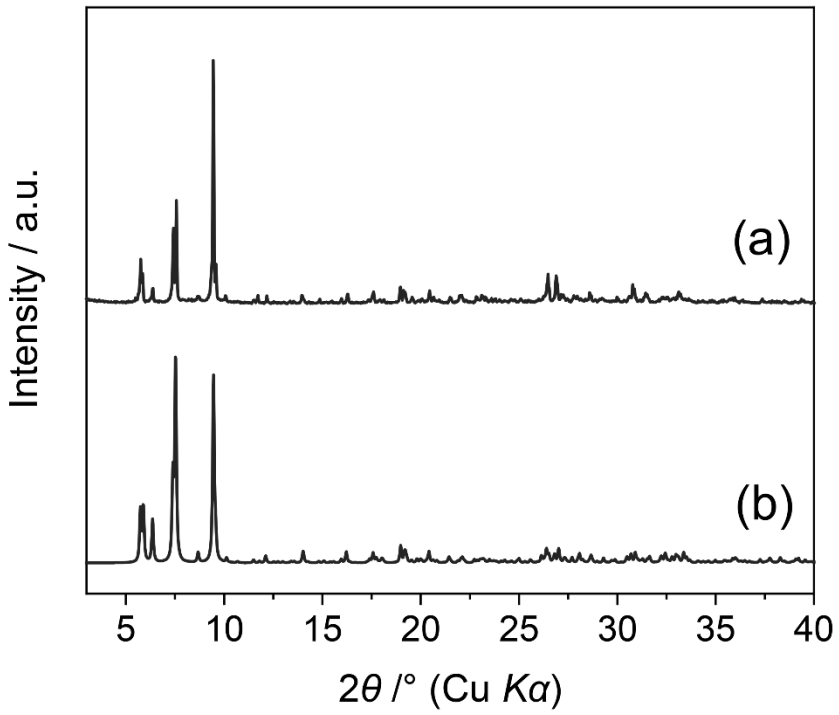

Fig. S9 PXRD patterns of **$Al_{28}V_4$-PW_9V_3**. (a) Experimental and (b) simulated from the CIF file.

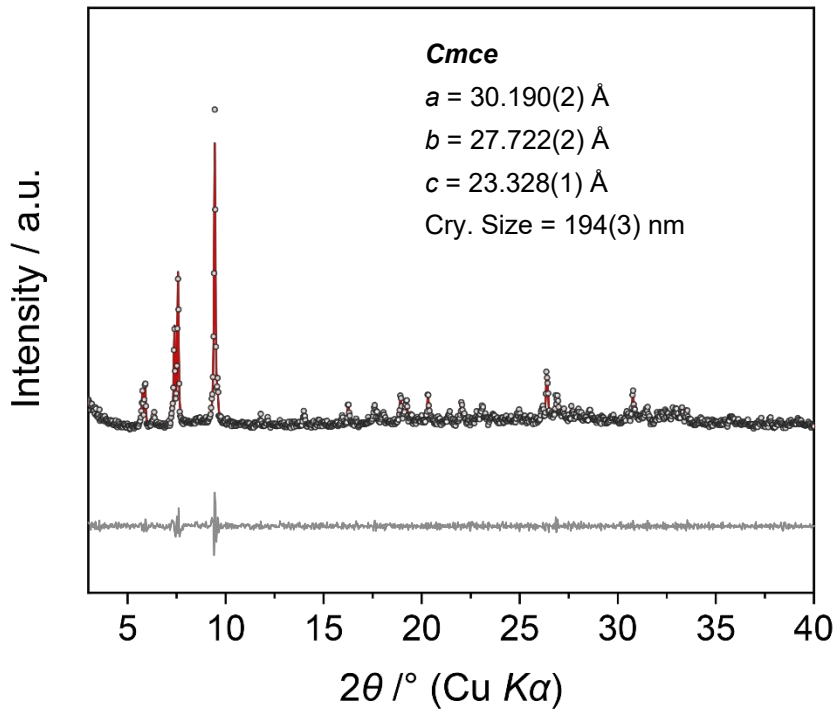

Fig. S10 Experimental (open circles) and calculated (red solid line) PXRD patterns of **$Al_{28}V_4$-PW_9V_3** by the Le Bail method. The bottom line shows the difference profile.

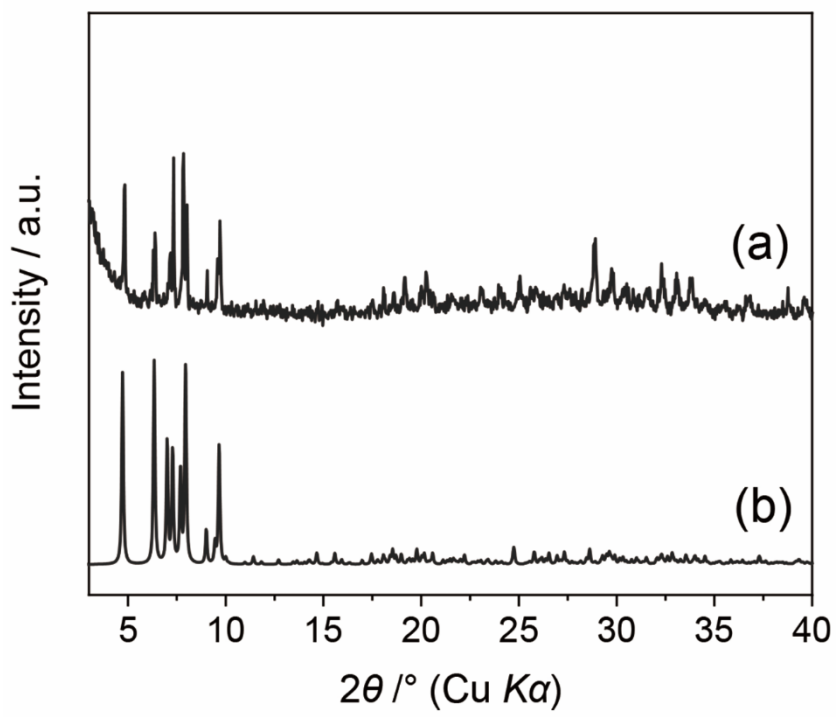

Fig. S11 PXRD patterns of **δ-Al$_{13}$-PW$_9$V$_3$**. (a) Experimental and (b) simulated from the CIF file.

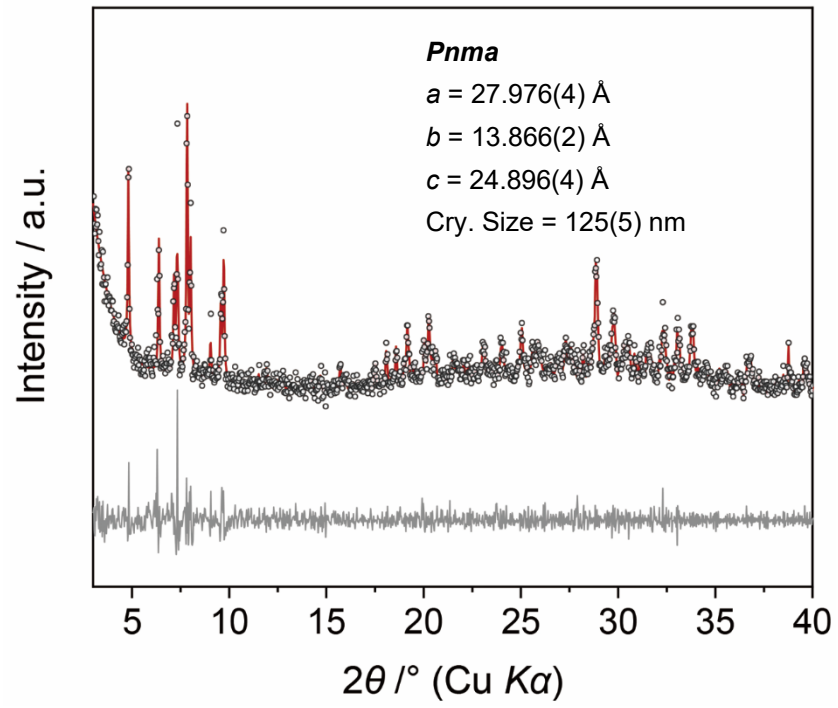

Fig. S12 Experimental (open circles) and calculated (red solid line) PXRD patterns of **δ-Al$_{13}$-PW$_9$V$_3$** by the Le Bail method. The bottom line shows the difference profile.

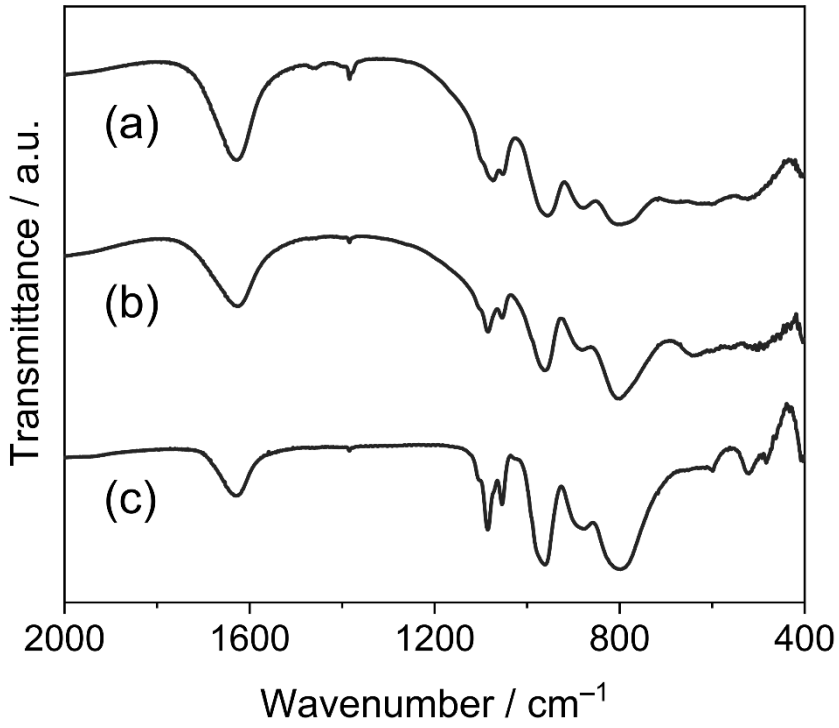

Fig. S13 IR spectra of (a) **$Al_{28}V_4$-PW_9V_3**, (b) **δ-Al_{13}-PW_9V_3** and (c) $K_6PW_9V_3O_{40}\cdot nH_2O$. **$Al_{28}V_4$-$PW_9V_3$**: 1073 ν_{asym}(V=O, P−O), 1051 ν_{sym}(V=O, P−O), 955 ν(W=O), 878 ν(W−O_c−W), 797 ν(W−O_e−W, Al-O_{Td}), 631 ν(Al−OH_{Oh}) 523 ν(Al−OH_{Oh}) ,465 ν(Al-OH_{2Oh}). **δ-Al_{13}-PW_9V_3**: 1084 ν_{asym}(V=O, P−O), 1054 ν_{sym}(V=O, P−O), 964 ν(W=O), 884 ν(W−O_c−W), 799 ν(W−O_e−W, Al-O_{Td}), 642 ν(Al−OH_{Oh}), 551 ν(Al−OH_{Oh}), 441 ν(Al-OH_{2Oh}).

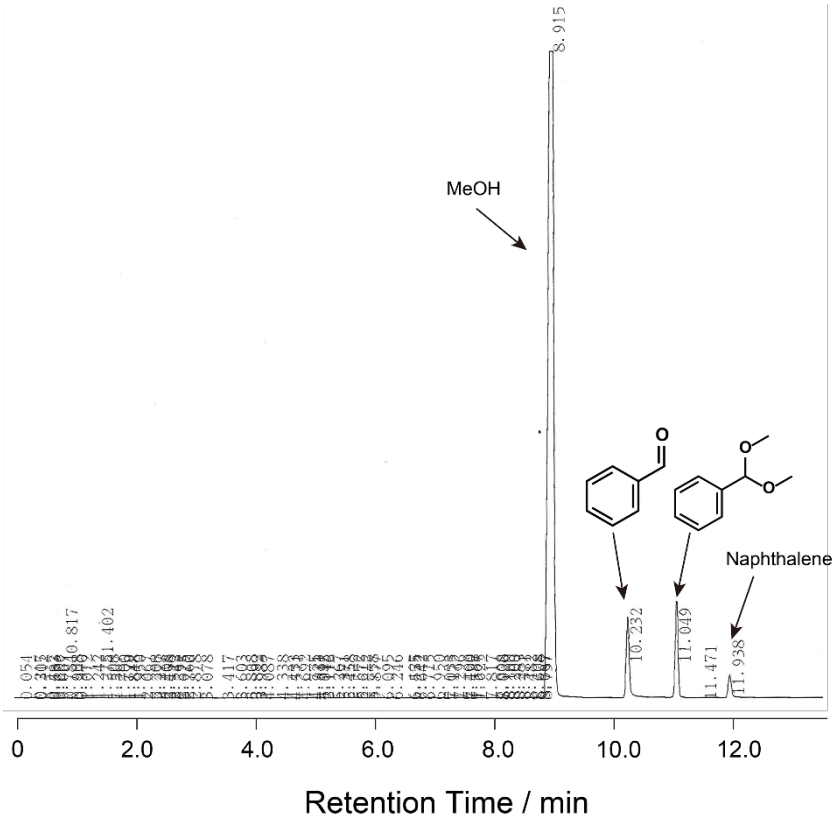

Fig. S14 GC chart of the acetalization of benzaldehyde with methanol catalyzed by $Al_{28}V_4$-PW_9V_3. The retention times of methanol, benzaldehyde, benzaldehyde dimethyl acetal, and naphthalene are 8.9, 10.2, 11.0, and 11.9 min, respectively. Reaction conditions: benzaldehyde (0.4 mmol), naphthalene (0.1 mmol), and catalyst (0.006 mmol) in 2 mL methanol at 343 K for 2 h.

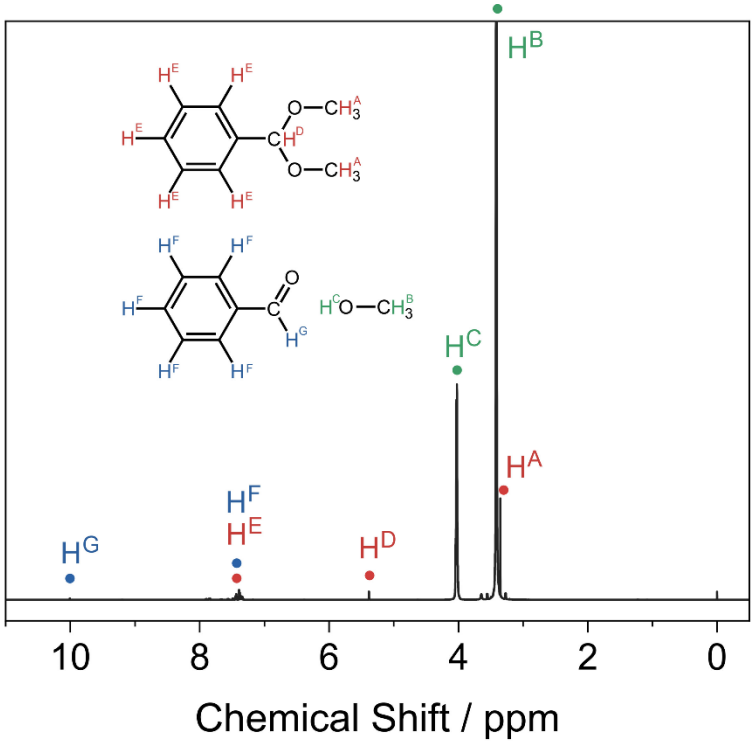

Fig. S15 Solution ^{1}H-NMR spectrum ($CDCl_3$) of the filtrate after the acetalization of benzaldehyde with methanol catalyzed by **$Al_{28}V_4$-PW_9V_3**. The signals labelled by red, blue, and green circles correspond to benzaldehyde dimethyl acetal, benzaldehyde, and methanol respectively. The small signals close to 8 ppm are those of naphthalene as an internal standard. Reaction conditions: benzaldehyde (0.4 mmol), naphthalene (0.1 mmol), and catalyst (0.006 mmol) in 2 mL methanol at 343 K for 2 h.

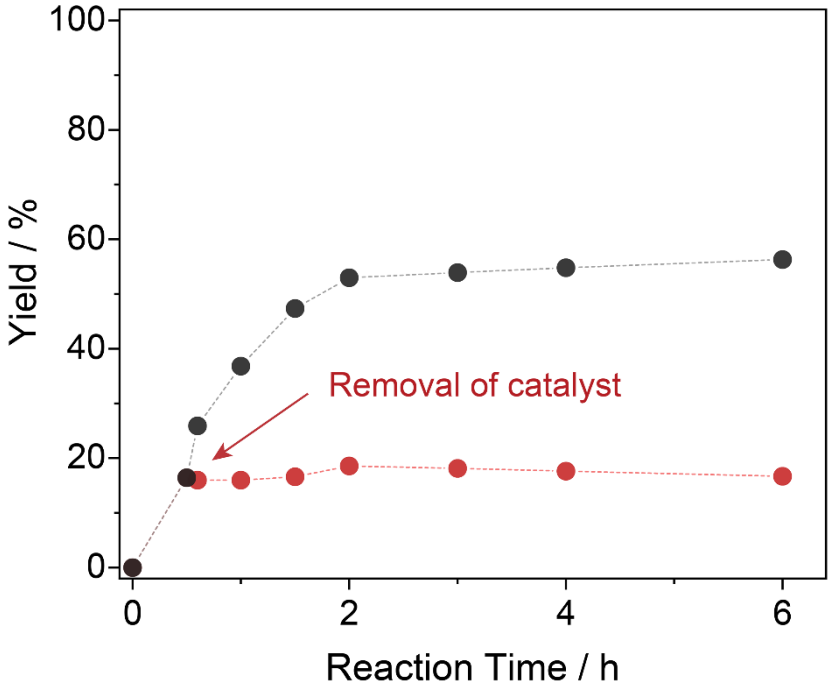

Fig. S16 Time courses of acetalization catalyzed by $\mathbf{Al_{28}V_4\text{-}PW_9V_3}$ at 343 K (black) and after removal of the catalyst (red).

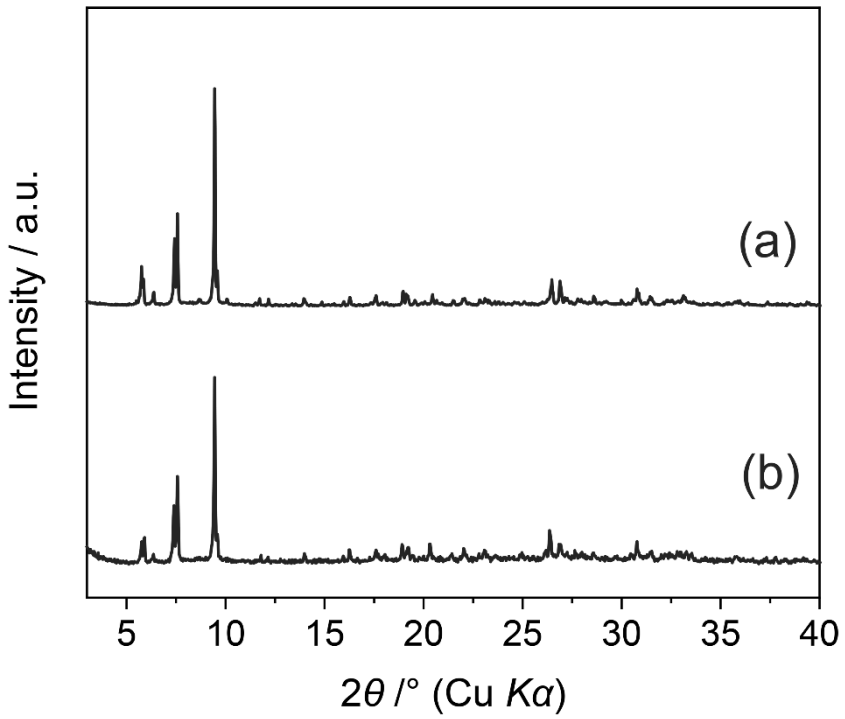

Fig. S17 PXRD patterns of **$Al_{28}V_4$-PW_9V_3**. (a) As synthesized and (b) after reaction.

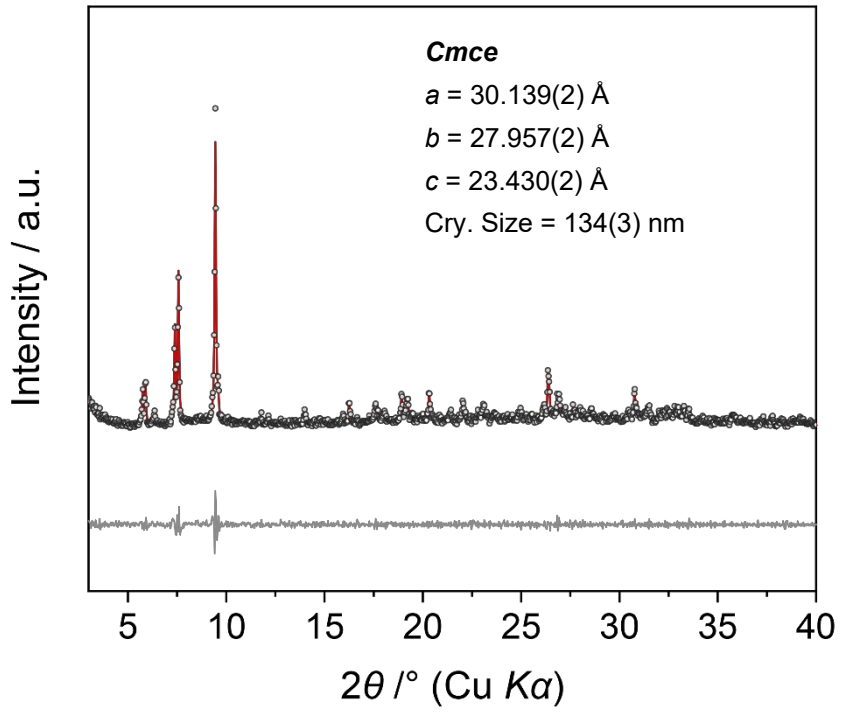

Fig. S18 Experimental (open circles) and calculated (red solid line) PXRD patterns of **$Al_{28}V_4$-PW_9V_3** after reaction by the Le Bail method. The bottom line shows the difference profile.

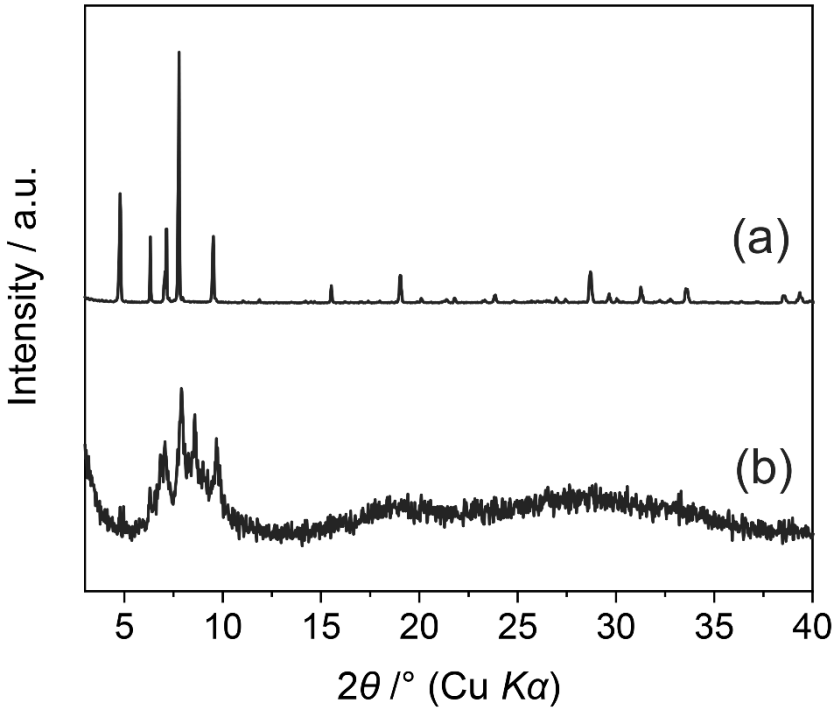

Fig. S19 PXRD patterns of **δ-Al$_{13}$-PW$_9$V$_3$**. (a) As synthesized and (b) after reaction.

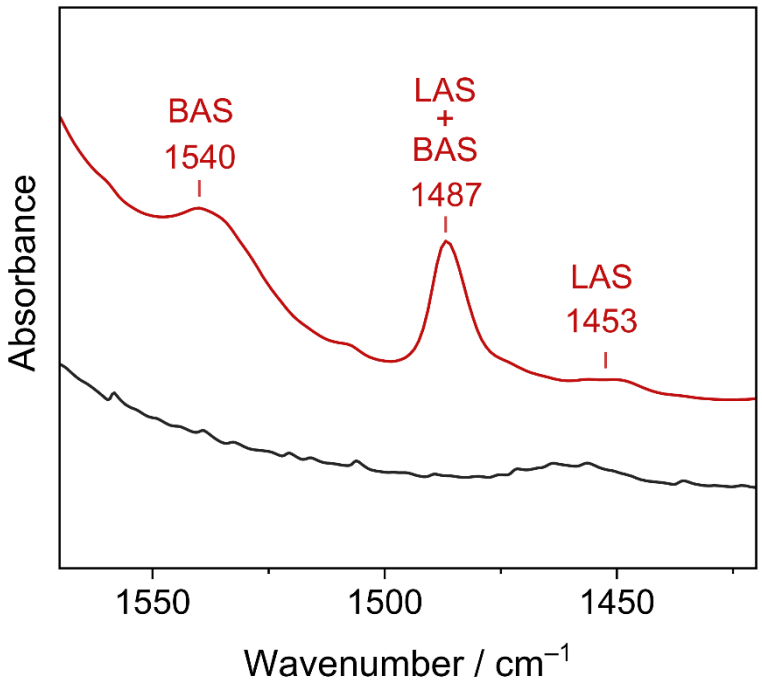

Fig. S20 IR spectra of pristine (black) and pyridine-treated (red) **Al$_{28}$V$_4$-PW$_9$V$_3$**. BAS: pyridine adsorbed on Brønsted acid site; LAS: pyridine adsorbed on Lewis acid site.

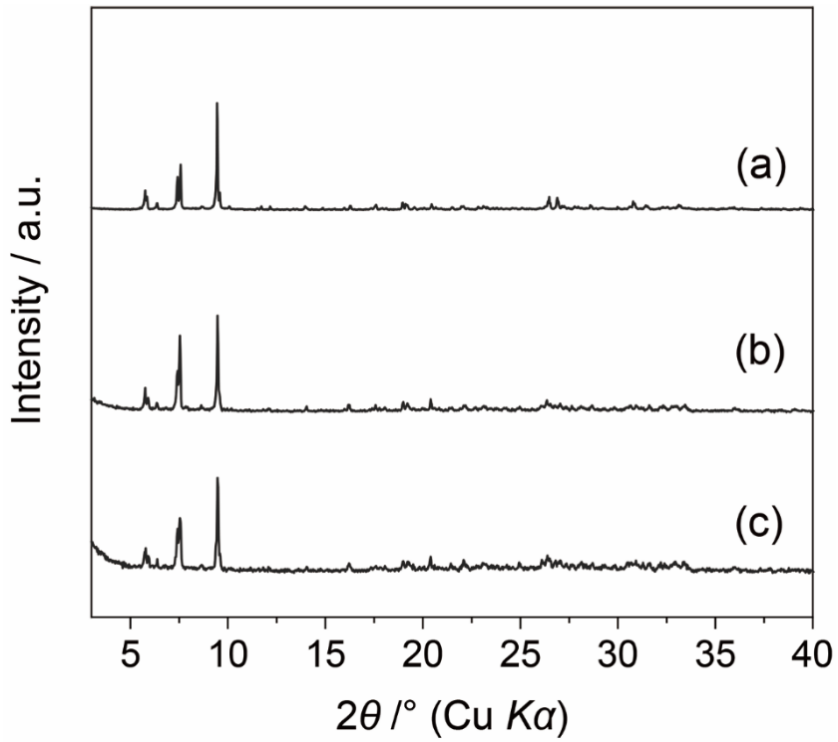

Fig. S21. PXRD patterns of $\mathbf{Al_{28}V_4\text{-}PW_9V_3}$: (a) pristine and treated with (b) 2,6-lutidine or (c) pyridine.

References

1 W. Zhou, N. Ogiwara, Z. W. Weng, C. C. Zhao, L. K. Yan and S. Uchida, *Chem. Commun.*, 2021, **57**, 8893−8896.

2 P. J. Domaille, *J. Am. Chem. Soc*., 1984, **106**, 25, 7677–7687.

3 G. M. Sheldrick, *Acta Crystallogr., Sect. A: Found. Adv.*, 2015, **71**, 3–8.

4 G. M. Sheldrick, *Acta Crystallogr., Sect. C: Struct. Chem.*, 2015, **71**, 3–8.

5 O. V. Dolomanov, L. J. Bourhis, R. J. Gildea, J. A. K. Howard and H. Puschmann, *J. Appl. Crystallogr.*, 2009, **42**, 339–341.

6 A. L. Spek, *Acta Crystallogr., Sect. C: Struct. Chem.*, 2015, **71**, 9–18.

7 A. Altomare, C. Cuocci, C. Giacovazzo, A. Moliterni, R. Rizzi, N. Corriero, and A. Falcicchio, *J. Appl. Cryst.*, 2013, **46**, 1231–1235.

8 J. -H. Son, Y. -U. Kwon, *Inorg. Chim. Acta*., **2005**, *358*, 310−314.

9 S. Hayashi and K. Hayamizu, *Bull. Chem. Soc. Jpn*., **1990**, *63*, 961–963.

10 M. J. Frisch, G. W. Trucks, H. B. Schlegel, G. E. Scuseria, M. A. Robb, J. R. Cheeseman, G. Scalmani, V. Barone, B. Mennucci, G. A. Petersson, H. Nakatsuji, M. Caricato, X. Li, H. P. Hratchian, A. F. Izmaylov, J. Bloino, G. Zheng, J. L. Sonnenberg, M. Hada, M. Ehara, K. Toyota, R. Fukuda, J. Hasegawa, M. Ishida, T. Nakajima, Y. Honda, O. Kitao, H. Nakai, T. Vreven, J. A. Jr. Montgomery, J. E. Peralta, F. Ogliaro, M. Bearpark, J. J. Heyd, E. Brothers, K. N. Kudin, V. N. Staroverov, T. Keith, R. Kobayashi, J. Normand, K. Raghavachari, A. Rendell, J. C. Burant, S. S. Iyengar, J. Tomasi, M. Cossi, N. Rega, J. M. Millam, M. Klene, J. E. Knox, J. B. Cross, V. Bakken, C. Adamo, J. Jaramillo, R. Gomperts, R. E. Stratmann, O. Yazyev, A. J. Austin, R. Cammi, C. Pomelli, J. W. Ochterski, R. L. Martin, K. Morokuma, V. G. Zakrzewski, G. A. Voth, P. Salvador, J. J. Dannenberg, S. Dapprich, A. D. Daniels, O. Farkas, J. B. Foresman, J. V. Ortiz, J. Cioslowski and D. J. Fox, *Gaussian 09, Rev. D.01*; Gaussian, Inc.: Wallingford, CT, 2013.

11 (a) A. D. Becke, *J. Chem. Phys.*, 1993, **98**, 5648–5652. (b) C. Lee, C. Yang and R. G. Parr, *Phys. Rev. B: Condens. Matter Mater. Phys.*, 1988, **38**, 785–789.

12 (a) M. M. Francl, W. J. Pietro, W. J. Hehre, J. S. Binkley, M. S. Gordon, D. J. Defrees and J. A. Pople, *J. Chem. Phys.*, **1982**, *77*, 3654–3665. (b) P. C. Hariharan and J. A. Pople, *Theor. Chem. Acc.*, 1973, **28**, 213–222. (c) G. A. Petersson, T. G. Tensfeldt and J. A. Montgomery, *J. Chem. Phys.*, 1991, **94**, 6091–6101.

13 P. J. Hay and W. R. Wadt, *J. Chem. Phys.*, 1985, **82**, 299–310.

14 J. Tomasi, B. Mennucci and R. Cammi, *Chem. Rev*., 2005, **105**, 2999–3093.

15 I. D. Brown and D. Altermatt, *Acta Crystallogr.*, 1985, **B41**, 244–247.